Characterization of unintentional doping in localized epitaxial GaN layers on Si wafers by scanning spreading resistance microscopy

Thomas Kaltsounis, Helge Haas, Matthieu Lafossas, Simona Torrengo, Vishwajeet Maurya, Julien Buckley, Denis Mariolle, Marc Veillerot, Alain Gueugnot, Laurent Mendizabal, et al.

Characterization of unintentional doping in localized epitaxial GaN layers on Si wafers by scanning spreading resistance microscopy

Thomas Kaltsounis [1, 2], Helge Haas [1], Matthieu Lafossas [1], Simona Torrengo [1], Vishwajeet Maurya [1], Julien Buckley [1], Denis Mariolle [1], Marc Veillerot [1], Alain Gueugnot [1], Laurent Mendizabal [1], Yvon Cordier [2] and Matthew Charles [1]

[1]*Univ. Grenoble Alpes, CEA, LETI, 38000 Grenoble, France*
[2]*Univ. Côte d'Azur, CNRS, CRHEA, 06560 Valbonne, France*

Abstract

Localized epitaxy of gallium nitride (GaN) on silicon (Si) is studied, with the aim of achieving material compatible with 1200 V vertical devices, in particular an unintentional doping level less than 1 x 10^{16} cm^{-3}, which is essential to have high quality devices. In this study, three mask materials (SiN, SiO_2, Al_2O_3) are examined and the unintentional doping concentration in GaN layers grown by metal organic vapor phase epitaxy (MOVPE) is investigated by scanning spreading resistance microscopy (SSRM). The results from SSRM are verified by secondary ions mass spectroscopy (SIMS) and show that an unintentional doping concentration lower than 10^{16} cm^{-3} is achieved when Al_2O_3 is used as the mask material. This value is lower than any previous studies of localized GaN growth, and in addition, this is the first time that SSRM has been used to observe such low doping concentrations in GaN.

Keywords

Localized epitaxy, GaN-on-Si, unintentional doping, scanning spreading resistance microscopy

1. Introduction

High power electronics concern devices capable of efficient conversion and control of electrical power, typically above 1kW. Over the past few decades, Si-based transistors have dominated in this field. However, wide-bandgap semiconductors, such as GaN, appear to be the perfect materials to overtake Si and prevail in future electronic applications. [1], [2] Its large energy gap and maximum electric field allows GaN-based devices to achieve higher breakdown voltages (BV) and operate at voltages 11 times higher than their Si-based counterparts, for a given thickness. Moreover, GaN-based devices are able to operate at temperatures higher than 300°C, which is twice the maximum of those for Si-based devices [3], [4] in spite of a similar thermal conductivity for silicon and GaN grown on silicon. [5] These characteristics, along with the excellent transport properties, lead to an improvement in the trade-off between specific R_{on} (on-resistance for a given surface area) and BV. This means that the components can be smaller, and so potentially cheaper. Silicon carbide can achieve similar benefits to GaN, but the high cost of wafers means that GaN on 200 mm-diameter Si remains an extremely attractive option.

Due to the high cost of GaN wafers, their varying quality and their limited availability, the search for alternative materials to serve as substrates is imperative. The low wafer and epitaxy cost, along with the low technological barriers to process large-diameter wafers, make Si substrates an excellent alternative to the native GaN. In addition, Si has good thermal and electrical conductivity, compared to other low-cost foreign substrates, for example sapphire. However, the large lattice mismatch between GaN and Si results in structural defects and a high density of dislocations in the grown GaN layer. [6]

For the growth of GaN on Si, buffer layers are required, firstly, because of the meltback etching effect [7] between them, and, secondly, in order to control the strain imposed during cooling from growth

temperature, due to the difference in thermal expansion coefficient between GaN and Si. [8] During the growth, the buffer layers, AlN and AlGaN, introduce a compressive strain to the GaN layer, resulting in a strong convex bow. When the structure is cooled down to room temperature, a large tensile stress is generated in the nitride layers, due to the thermal expansion coefficient mismatch, and if the growth is well controlled, the wafer becomes flat at room temperature. [9] For thicker layers, the GaN relaxes, and it is not possible to keep sufficient compression in the layers. This limits the thickness of GaN layers, that can be grown on planar Si wafers, to 7 µm but the wafers are more fragile. Localized epitaxial growth relaxes this tensile stress elastically, and enables the growth of thicker GaN layers. [10], [11]

These thicker GaN layers can be used for the fabrication of vertical power devices. Vertical devices are more compact than lateral devices, and they have no need for high carbon doping, improving their dynamic performance. [1] Furthermore, the electric field is more uniform and the current distribution is more spread, making the thermal management of vertical devices easier. [12] For vertical power devices operating at voltages higher than 1 kV, a drift layer of thickness 10 µm, with a low doping concentration in the order of 10^{16} cm^{-3} is required. [13]

In localized GaN growth, Ga atoms diffuse on the mask towards the mask openings. There are two effects from this diffusion. Firstly, after nucleation in the openings, growth extends both laterally to cover a part of the mask at the edge of the opening and vertically (superelevations), meaning that the thickness of the GaN layer is higher at the areas adjacent to the mask openings, than at the center. This phenomenon is dependent on the growth conditions and duration but also on the mask area surrounding the opening with a limit related to the diffusion length of Ga. In addition, the Ga atoms slightly etch the mask, which can incorporate Si or oxygen (O) atoms from the mask to the grown layer, elements that are good n-type dopants of GaN. As a result, there is an unintentional doping in the GaN layer. This has been previously reported for GaN on sapphire growth, where the lowest unintentional doping of GaN of 5 x 10^{16} cm^{-3} was found using an Al_2O_3 mask. [10]

In this study, the effects of three mask materials (SiO_2, SiN, Al_2O_3) in the unintentional doping concentration of the localized epitaxial GaN layers are investigated. SSRM is employed as the characterization technique on specially prepared cross-sections of the growth structures to give detailed spatial doping information. These SSRM results are then verified by SIMS.

2. Experimental Section

Growth was carried out on a single-wafer AIXTRON Crius-R200 MOVPE tool, using 200 mm-diameter Si-wafers. The buffer layers, AlN and AlGaN, an undoped GaN layer of 300 nm and an 800 nm-thick n-GaN layer with doping concentration of 5 x 10^{18} cm^{-3}, serving as the template, were grown on the planar wafers. Afterwards, the deposition of the 50 nm-thick mask followed, by low-pressure chemical vapor deposition at 750 °C for SiN, plasma enhanced chemical vapor deposition at 400 °C for SiO_2 and atomic layer deposition at 300 °C for Al_2O_3. The patterning of the mask by reactive ion etching followed and finally, the localized growth of GaN was performed.

For this study, two different structures were grown, employing SiN, SiO_2 or Al_2O_3 as the growth mask for each structure, resulting in 6 samples. The first set of samples had one nominally 1.5 µm-thick non-intentionally doped (nid) GaN layer grown at 1040 °C, with a nominal growth rate of 1.5 µm/h (for full wafer growth). The pressure in the chamber was 400 mbar and the NH_3 flow was 10 slm. In the second set of samples, four nominally 0.75 µm-thick GaN layers were grown, each one having a different intentional doping concentration. Starting from the first layer grown, the four doping concentrations were 5 x 10^{18} cm^{-3}, 5 x 10^{17} cm^{-3}, 5 x 10^{16} cm^{-3} and nid, with the doping level estimated from full wafer 2D growth. The growth rate of these layers was 1.5 µm/h (for full wafer growth). The dopant used was Si, and the precursors for silicon and gallium were silane (SiH_4) and tri-methyl gallium (TMGa) respectively.

To prepare the samples for the SSRM measurements, they were first cleaved and then the cross-sections were prepared. The cross-sections of the first set of samples were prepared by mechanical polishing on the cleaved area, while the cross-sections of the samples of the second set were prepared by ionic polishing in a Leica TIC-3X tool.

SSRM is an excellent technique for the study of doping concentration within GaN-based layers. [14] It is based on atomic force microscopy (AFM), however since it is conducted in contact mode and high forces are applied to the tip, doped-diamond-coated probes are used. In addition, these probes assist in the penetration of the oxide layer, which typically forms rapidly on the surface. [15] The small conductive tip measures the local spreading resistance, which is directly proportional to the local resistivity. A bias voltage is applied between a back contact and the tip, in order to measure the current flowing through the sample. [16] SSRM is capable of measuring resistance in both high- and low-doped semiconducting regions, by employing a logarithmic amplifier with a current range from 10 pA to 0.1 mA. [15] The back contact on the samples was created by applying silver paint to the n-GaN bottom layer. All the measurements were conducted in air on a Bruker Dimension ICON AFM tool at atmospheric pressure. The applied DC sample bias was -2 and -6 V for the top-view and cross-section measurements on the samples of the first set respectively. The measurements on the samples of the second set were conducted under a DC sample bias of -8 V, as this gave clearer results.

SIMS measurements were performed on magnetic sector instrument considering a cesium source for primary ion beam. Negative polarity secondary ions were collected, in a high mass resolution configuration, in order to accurately monitor $^{28}Si^-$ independently of the $^{14}N_2^-$ contribution.

3. Results & Discussion

For this study, no mask was designed specifically for the localized epitaxy of GaN but an existing one was used. The measurements were carried out on three circular patterns on all the samples. Figure 1(a) shows a schematic of the three circular patterns under study. The first is a 5 mm-diameter circle and it will be referred to as Pattern A. The latter two have a diameter of 90 μm, but the mask distance between their edge and the outer rectangle, was 10 μm (Pattern B) and 20 μm (Pattern C) respectively, thus changing the amount of diffusive material arriving on the pattern. The center of the 5 mm-diameter circle behaves like a planar substrate and provides a reference for evaluating the difference of the doping concentration between the center and the edge, as a result from the diffusion of the Ga atoms on the mask. Figure 1(b) shows a scanning electron microscopy (SEM) image of the area including the two latter patterns. After the growth, the structures have developed a hexagonal shape. This happens because when GaN, with its hexagonal crystalline structure, is grown in a c-plane (0001) direction, it develops a hexagonal structure. [17] The superelevations are visible too, particularly on the structures with larger diffusive areas. The mask material will be used as the reference to describe the samples.

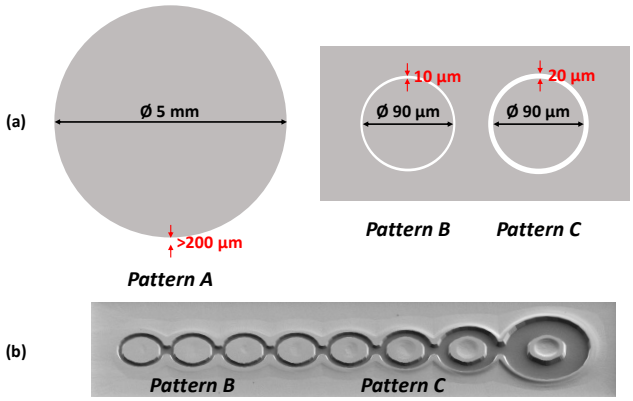

Figure 1. (a) Schematic showing the three circular patterns under study. Pattern A is the 5 mm-diameter circle, Pattern B is the 90 µm-diameter circle with diffusion distance of 10 µm and Pattern C is the 90 µm-diameter circle with diffusion distance of 20 µm. The black arrows show the diameters of the patterns and the red arrows the diffusion distance around them, (b) SEM image of the 90 µm-diameter structures with different diffusive areas around them on the Al_2O_3 mask sample of the second set. Pattern B and Pattern C are noted on the image. Al_2O_3 mask appears darker compared to GaN

Figure 2 shows the SSRM images of the top-view measurements at the center and the edge of Pattern A on the first set of samples, which had a single non-intentionally doped GaN layer. The features observed in the images are the atomic steps on the GaN surface where the resistance is modified due to a change in the contact area with the tip. The resistivity at the center of the circle on the SiO_2 and SiN mask samples is higher than that at the edge. Consequently, the doping concentration at the edge of the structure is higher. This difference is due to the unintentional doping. In the case of the Al_2O_3 mask sample, no signal is obtained, which implies that the resistivity of the layer is too high to measure.

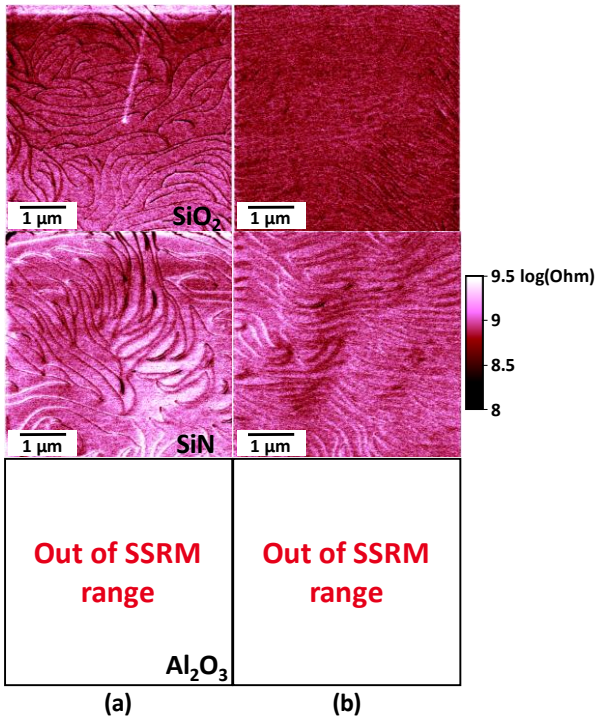

Figure 2. Top-view SSRM measurements on Pattern A on the SiN, SiO_2 and Al_2O_3 mask samples of the first set at the (a) center and (b) edge of the pattern

In order to try to quantify the doping in these layers, cross-sections were prepared of the edge of Pattern B, on the SiO_2 and Al_2O_3 mask samples. These were examined and the SSRM images are shown in Figure 3. The images, especially that of the Al_2O_3 mask sample, may not be extremely clear, due to surface damage due to mechanical polishing, during the cross-section preparation. However, it is still possible to draw some conclusions regarding the resistance of the layers. On the SiO_2 mask sample, the nid layer shows almost the same resistivity as the bottom n-GaN layer, thus, its doping concentration is around 5 x 10^{18} cm^{-3}. This is several orders of magnitude too high for the fabrication of vertical power components. On the other hand, the SSRM measurement on the Al_2O_3 mask sample shows that no signal is obtained from the area where the nid layer is supposed to be. As the sample with Al_2O_3 mask is too resistive to measure, this is promising for device fabrication, but it was necessary to push the SSRM further in order to quantify the doping in these layers.

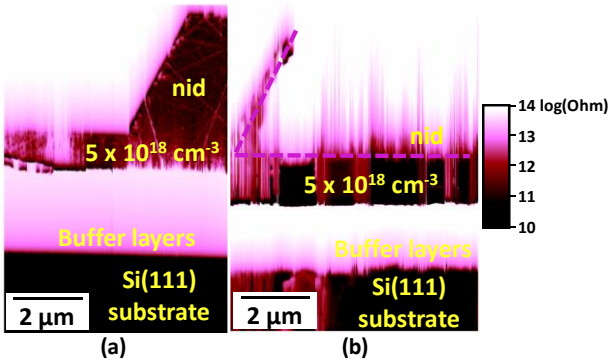

Figure 3. SSRM measurements on the cross-section of the edge of Pattern B on the (a) SiO_2 and (b) Al_2O_3 mask sample of the first set

The second set of samples, where the intentionally-doped layers can be used as a reference, are therefore well adapted to calibrate the SSRM measurements. Figure 4 shows the SSRM measurements on the cross-sections of the edge of Pattern B on all samples and Figure 5 shows those of Pattern C. For the SiN mask samples, all the intentionally doped layers appear to have roughly the same resistivity, the same as for the bottom n-GaN layer grown before patterning. For the nid layer in both figures, although it shows a higher resistivity, the AFM images, obtained during the SSRM measurements, show that on this area there is a change in the morphology of the surface, perhaps due to the preparation of the cross-section. This has not been fully understood, but it would be extremely surprising for the nid sample to have significantly higher resistivity than the layer with a nominal doping of 5 x 10^{16} cm^{-3}. The SSRM measurement on the SiO_2 mask samples gives a similar result. All of the layers are roughly the same color, with the exception of a thin top layer which has a higher resistivity. This layer does not correspond to the whole nid layer, but once again corresponds to a difference in morphology seen by AFM. Once again, we attribute this change in resistivity to the morphology, and we consider that the nid layer has a very similar doping level to the other intentionally doped layers.

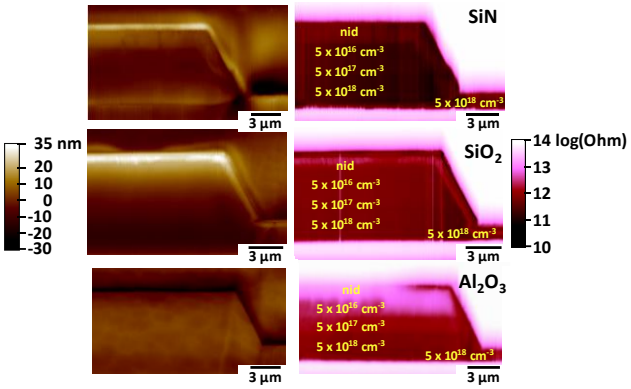

Figure 4. Left column: AFM images in contact mode on the cross-section of the edge of Pattern B on the SiN, SiO_2 and Al_2O_3 mask samples of the second set, Right column: SSRM measurements on the same area, with nominal intentional doping of each layer labelled in yellow

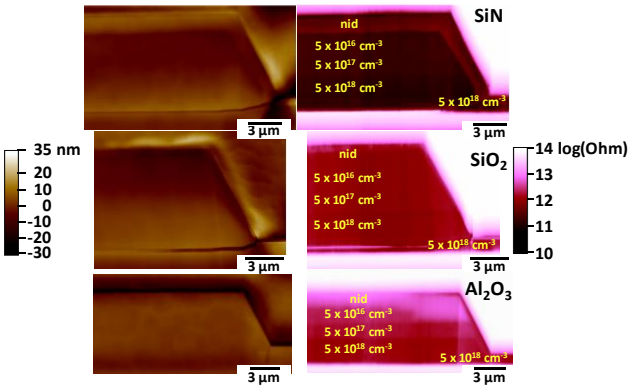

Figure 5. Left column: AFM images in contact mode on the cross-section of the edge of Pattern C on the SiN, SiO_2 and Al_2O_3 mask samples of the second set, Right column: SSRM measurements on the same area, with nominal intentional doping of each layer labelled in yellow

In the case of the Al_2O_3 mask sample, all four layers can be clearly distinguished. The layer of nominal doping concentration 5 x 10^{18} cm^{-3} appears to be slightly more resistive than the n-GaN layer grown before patterning, hence it has a doping concentration slightly lower than 5 x 10^{18} cm^{-3}. This is likely due to additional Ga diffusing from the mask, and so diluting the dopant atoms. For the next layers, the resistivity gradually increases, as expected, since the doping concentration of each layer decreases. Furthermore, the AFM image shows a smooth surface, with no changes in the morphology of the surface. Unlike the other two samples, the unintentional doping in the structure is extremely low.

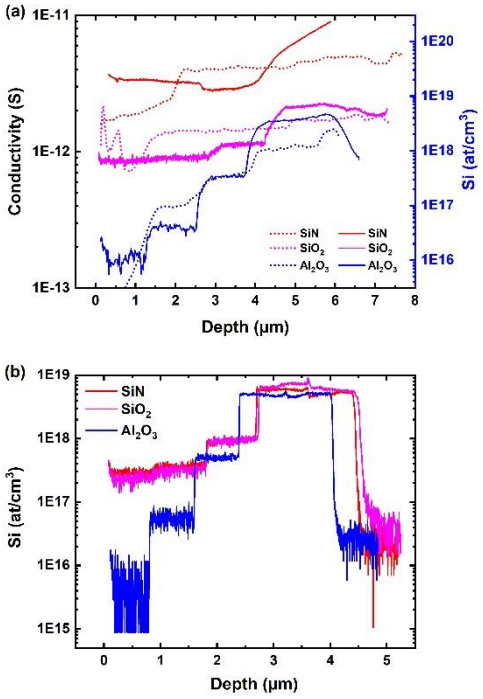

Figure 6. (a) Dotted lines: Conductivity of Pattern B, Solid lines: SIMS measurements of Si on the same structure on the SiN, SiO_2 and Al_2O_3 mask samples of the second set (b) SIMS measurements of Si on Pattern A on the SiN, SiO_2 and Al_2O_3 mask samples of the second set

In order to validate the SSRM measurements, and in particular to examine the concentration of Si, SIMS measurements were carried out at the center of Pattern B and at the center of Pattern A for the three samples of the second set.

Figure 6(a) shows the conductivity profiles extracted from the SSRM measurements as dotted lines and the SIMS measurements of Si concentration on Pattern B as solid lines. The SiN and SiO_2 mask samples show similar conductivity profiles, as expected from the images in Figure 4, with both showing roughly constant conductivity throughout the structure, apart from near the surface where we suggest that the conductivity is altered by the surface morphology due to the sample preparation. We do not find the same absolute values for the nGaN layer before patterning, which shows the limitations of SSRM, but as relative measurements, calibration samples such as these can give quantitative data. For the Al_2O_3 mask sample, the conductivity profile shows clear step evolution, as seen in the images of Figure 4. In addition, we can note that the nid layer does not show a constant conductivity, but it decreases towards the top.

The SIMS measurements show the same trends. The Si concentration in the SiN mask sample is very high, starting from 10^{19} cm^{-3} for the first two layers and then increasing to 2 x 10^{20} cm^{-3}. Although, it is possible that, in this concentration, there is Si coming from the mask, it is not expected to be lower than 5 x 10^{18} cm^{-3}, as the electrical measurements show high conductivity. On the SiO_2 mask sample, the bottom n-GaN and the first regrown layer have a Si concentration of 6 x 10^{18} cm^{-3}. The other layers have high Si concentrations, of the order of 10^{18} cm^{-3}, suggesting that Si is coming from the mask to cause unintentional doping. The SIMS measurement of the structure on the Al_2O_3 mask sample verifies that there is no unintentional doping in the structure, since the Si concentration in each layer agrees with the nominal values. The measurement on the nid layer is noisy but it shows a low Si concentration of low 10^{16} cm^{-3}. This is at the detection limit reachable for the SIMS measurement in this experimental context, and is therefore consistent with very high resistivity observed.

Figure 6(b) shows the SIMS measurements performed at the center of Pattern A for all three samples. This time, the signal is much clearer, as there can be no interference from the mask, and we see that for the SiN and SiO_2 mask samples the unintentional doping remains high. Apart from the first two regrown layers, where the Si concentration is about 5 x 10^{18} cm^{-3} and 10^{18} cm^{-3} respectively in both samples, the other two layers have a Si concentration between 3 x 10^{17} cm^{-3} and 5 x 10^{17} cm^{-3}. These concentrations are at least one order of magnitude higher than the nominal values. Therefore, the unintentional doping concentration in both cases is higher than 10^{17} cm^{-3}. On the Al_2O_3 mask sample, the SIMS measurement shows a profile similar to that for Pattern B but the Si concentration of the nid layer is lower, and a silicon concentration of 5 x 10^{15} cm^{-3} has been achieved. This was to be expected because there is no obvious source of silicon with an Al_2O_3 mask.

The carbon and oxygen concentrations were also investigated by SIMS, as they can act as dopants of GaN. As can been seen in the Figures S1 and S2 of the appendix, in the case of Pattern B on the SiN and SiO_2 mask samples, their concentration is higher than 10^{18} cm^{-3}. On the Al_2O_3 mask sample, the carbon concentration is lower than 5 x 10^{16} cm^{-3}, whereas that of O is 10^{18} cm^{-3} in the nid layer and it decreases in the other layers. The profiles of this pattern are hard to interpret, as there may be some material being sputtered from the masks, thus further study is required for the understanding of the doping concentration. In Pattern A, the concentrations of both elements are lower than 10^{17} cm^{-3}. In particular, on the Al_2O_3 mask sample, the carbon concentration is about 4 x 10^{16} cm^{-3} and the oxygen concentration is 5 x 10^{16} cm^{-3}. This suggests that the doping concentration of the epitaxial layers is dominated by Si.

From these analyses, we can see that SiN and SiO_2 are not suitable as mask materials for the localized growth of GaN on Si wafers, for vertical power devices because of the high unintentional doping concentrations. However, when comparing the SIMS data and the resistivity data of the layers with Al_2O_3 mask, we can see that we have achieved record values of non-intentional doped layers for localized growth of GaN, with a carrier concentration <1 x 10^{16} cm^{-3}.

Returning to Figure 4 and Figure 5, both the AFM and SSRM images, the thickness of the structure can be extracted, which is 6 µm for the layers of Pattern B, and nearly 7 µm for Pattern C. These values are larger than the "nominal" values from 2D growth due to the Ga atoms diffused from the mask onto the structures. In addition, the larger diffusion distance of 20 µm leads to increased thickness, again due to additional gallium diffusing from the mask. These islands show no cracking at the surface, showing good progress towards the desired 10 µm thick layers.

4. Conclusions

In this study, the unintentional doping concentration in localized grown GaN layers has been investigated, by employing three mask materials. When SiN and SiO_2 are the epitaxy masks, the diffusion of the Ga atoms causes an unintentional doping concentration in the GaN layers of the order of 10^{18} cm^{-3}. Such a doping concentration makes the fabrication of high quality vertical power devices impossible. However, for an Al_2O_3 mask, the unintentional doping in the GaN layers is extremely low. For the first time, we have shown that SSRM can be used to image GaN layers with a doping concentration of the order of 10^{16} cm^{-3}, and with this technique in combination with SIMS, we confirm that we have achieved layers with record low doping levels for localized growth of GaN, < 1 x 10^{16} cm^{-3}. These layers were uncracked structures up to 7 µm and so these are very promising steps towards the material properties required for 1200 V vertical devices by localized growth.

Acknowledgements

Part of this work, carried out on the Platform for Nanocharacterisation (PFNC), was supported by the 'Recherches Technologiques de Base' program.

References

[1] J. Hu, Y. Zhang, M. Sun, D. Piedra, N. Chowdhury, and T. Palacios, "Materials and processing issues in vertical GaN power electronics," *Mater. Sci. Semicond. Process.*, vol. 78, no. September 2017, pp. 75–84, 2018, doi: 10.1016/j.mssp.2017.09.033.

[2] F. Roccaforte *et al.*, "Barrier inhomogeneity in vertical Schottky diodes on free standing gallium nitride," *Mater. Sci. Semicond. Process.*, vol. 94, no. January, pp. 164–170, 2019, doi: 10.1016/j.mssp.2019.01.036.

[3] F. Iacopi, M. Van Hove, M. Charles, and K. Endo, "Power electronics with wide bandgap materials: Toward greener, more efficient technologies," *MRS Bull.*, vol. 40, no. 5, pp. 390–395, 2015, doi: 10.1557/mrs.2015.71.

[4] M. Meneghini *et al.*, "GaN-based power devices: Physics, reliability, and perspectives," *J. Appl. Phys.*, vol. 130, no. 18, 2021, doi: 10.1063/5.0061354.

[5] C. Mion, J. F. Muth, E. A. Preble, and D. Hanser, "Thermal conductivity, dislocation density and GaN device design," *Superlattices Microstruct.*, vol. 40, no. 4-6 SPEC. ISS., pp. 338–342, 2006, doi: 10.1016/j.spmi.2006.07.017.

[6] Y. Zhang and A. Dadgar, "Gallium nitride vertical power devices on foreign substrates : a review and outlook," 2018, doi: 10.1088/1361-6463/aac8aa.

[7] M. Khoury, O. Tottereau, G. Feuillet, P. Vennéguès, and J. Zúñiga-Pérez, "Evolution and prevention of meltback etching: Case study of semipolar GaN growth on patterned silicon substrates," *J. Appl. Phys.*, vol. 122, no. 10, 2017, doi: 10.1063/1.5001914.

[8] M. Meneghini *et al.*, *GaN-Based Lateral and Vertical Devices*. 2023. doi: 10.1007/978-3-030-79827-7_15.

[9] M. Charles *et al.*, " (Invited) Epitaxy of GaN on Si (111) for Power Electronics, RF and LEDs ," *ECS Trans.*, vol. 86, no. 7, pp. 233–247, 2018, doi: 10.1149/08607.0233ecst.

[10] A. Debald, S. Kotzea, J. Riedel, M. Heuken, H. Kalisch, and A. Vescan, "GaN Micropillar Schottky Diodes with High Breakdown Voltage Fabricated by Selective-Area Growth," *Phys. Status Solidi Appl. Mater. Sci.*, vol. 217, no. 7, pp. 2–9, 2020, doi: 10.1002/pssa.201900676.

[11] A. Tanaka, W. Choi, R. Chen, and S. A. Dayeh, "Si Complies with GaN to Overcome Thermal Mismatches for the Heteroepitaxy of Thick GaN on Si," *Adv. Mater.*, vol. 29, no. 38, pp. 1–6, 2017, doi: 10.1002/adma.201702557.

[12] Y. Zhang *et al.*, "Electrothermal simulation and thermal performance study of GaN vertical and lateral power transistors," *IEEE Trans. Electron Devices*, vol. 60, no. 7, pp. 2224–2230, 2013, doi: 10.1109/TED.2013.2261072.

[13] J. A. Cooper and D. T. Morisette, "Performance Limits of Vertical Unipolar Power Devices in GaN and 4H-SiC," *IEEE Electron Device Lett.*, vol. 41, no. 6, pp. 892–895, 2020, doi: 10.1109/LED.2020.2987282.

[14] A. Alberti *et al.*, *Measuring Techniques for the Semiconductor's Parameters*. 2023. doi: 10.1007/978-3-030-79827-7_4.

[15] R. A. Oliver, "Advances in AFM for the electrical characterization of semiconductors," *Reports*

Prog. Phys., vol. 71, no. 7, 2008, doi: 10.1088/0034-4885/71/7/076501.

[16] P. Eyben, M. Xu, N. Duhayon, T. Clarysse, S. Callewaert, and W. Vandervorst, "Scanning spreading resistance microscopy and spectroscopy for routine and quantitative two-dimensional carrier profiling," *J. Vac. Sci. Technol. B Microelectron. Nanom. Struct.*, vol. 20, no. 1, p. 471, 2002, doi: 10.1116/1.1424280.

[17] Q. Sun, C. D. Yerino, B. Leung, J. Han, and M. E. Coltrin, "Understanding and controlling heteroepitaxy with the kinetic Wulff plot: A case study with GaN," *J. Appl. Phys.*, vol. 110, no. 5, 2011, doi: 10.1063/1.3632073.